Vibration Suppression Study of Parallel Combined Damping Nonlinear Energy Sink on Piecewise Linear Systems

Xingke Qi[1], Jianchao Zhang[2]*, Jun Wang[1,2]

[1] Department of Mechanical Engineering, Shijiazhuang Tiedao University, Shijiazhuang 050043, Hebei, China
[2] State Key Laboratory of Mechanical Behavior and System Safety of Traffic Engineering Structures, Shijiazhuang Tiedao University, Shijiazhuang 050043, Hebei, China
DOI: 10.32629/aes.v4i4.1460

Abstract: The Nonlinear Energy Sink (NES) is a passive control device capable of achieving targeted energy transfer and effectively suppressing system vibrations. This paper conducts dynamic modeling and vibration suppression analysis of parallel combined damping nonlinear energy sinks in piecewise linear systems. Initially, the system's amplitude-frequency response curve is obtained using the harmonic balance method, validated by the Runge-Kutta method for accuracy. Subsequently, an analysis is performed on the vibration reduction capabilities of the parallel combined damping nonlinear energy sink and the influence of parameters on its vibration suppression effectiveness. Finally, the study investigates changes in the main system's maximum response amplitude with varying damping under different stiffness conditions and determines optimal parameter values based on trend analysis. Research findings indicate that the vibration reduction performance of the parallel combined damping nonlinear energy sink surpasses that of a single connected damping nonlinear energy sink. Furthermore, after parameter optimization, the main system achieves superior vibration reduction effects.
***Keywords*:** Nonlinear Energy Sink; Harmonic Balance Method; Vibration Reduction Performance; Parameter Optimization

1. Introduction

As a classic passive control device, the Nonlinear Energy Sink (NES) is characterized by its low cost, simple structure, and wide absorption bandwidth. It typically comprises a small mass block, viscous damping, and a highly nonlinear spring [1-3]. Under specific energy conditions, the NES can achieve unidirectional and irreversible energy transfer, maintaining a particularly high range of transfer efficiency—a phenomenon known as Targeted Energy Transfer (TET) [4-5]. Furthermore, when the system is subjected to harmonic excitation, the NES can exhibit Strongly Modulated Responses (SMR), significantly modulating the vibration amplitude of the main system, thereby achieving optimal vibration reduction effects [6-7]. With further advancements in NES research, scholars have introduced various novel NES structures, including orbital NES, bistable NES, lever-type NES, and nonsmooth NES [8-11].

Due to the complex nature of engineering environments and structural complexities, many scholars often simplify structures requiring vibration reduction to linear systems. They then couple these with the Nonlinear Energy Sink (NES) for analysis [12-14]. However, in practical engineering scenarios, systems requiring vibration reduction are not merely simple linear systems but rather more intricate nonlinear systems. Ji et al. [15] transformed the main system into a nonlinear system incorporating cubic stiffness and analyzed the steady-state response under various amplitude excitations. They introduced a linear absorber and found it effectively reduced vibrations in the nonlinear system, studying the absorber's parameters' impact on vibration suppression in the nonlinear system. Piccirillo [16] examined a main system consisting of segmented damping, segmented stiffness, and a mass block. Using a linear absorber, they suppressed chaotic responses in the nonlinear system, concluding conditions for converging chaotic responses in the system. Wang et al. [17] investigated the vibration suppression of a nonlinear energy sink on a self-excited system, discovering that under low-frequency harmonic excitation, the NES exhibited substantial vibration reduction effects on the self-excited system. These studies provided theoretical foundations for vibration reduction in nonlinear systems. Building upon this knowledge, this paper transforms the main system into a piecewise linear system and employs a parallel combined damping nonlinear energy sink to reduce vibrations in the main system.

Previously, scholars primarily focused on studying the influence of different NES structures on vibration suppression in the main system, paying less attention to the impact of the number of NES units on vibration reduction [18-20]. Consequently, there has been relatively little research analyzing the effect of the number of NES units. Song et al. [21] investigated the vibration suppression of parallel nonlinear energy sinks on the main system, finding that parallel nonlinear energy sinks could enhance system robustness without increasing mass. They also pointed out that the vibration reduction performance of parallel nonlinear energy sinks surpassed that of a single nonlinear energy sink. Zhang et al. [22] studied the effects of series-connected nonlinear energy sinks on vibration reduction in the main system. They discovered that series connections expanded the range of strongly modulated

responses in the main system. By comparing optimal energy spectra, they indicated that, compared to connecting a single nonlinear energy sink, series connections exhibited superior vibration reduction performance.

Although numerous scholars have conducted extensive research on NES systems, most of these studies have focused on individual NES units, lacking investigations into multi-stage NES systems. Furthermore, in the analysis process, the main system is often simplified into a linear system, which deviates significantly from actual scenarios. Due to these gaps in existing research, this paper establishes a dynamic model of a parallel combined damping NES for piecewise linear systems. Initially, the harmonic balance method is employed to solve the system's amplitude-frequency response, validated for accuracy using the Runge-Kutta numerical method. Subsequently, an analysis is conducted on the vibration reduction performance of the parallel combined damping NES and the influence of parameters on the main system's vibration suppression effects. Finally, variations in the maximum response amplitude of the main system under different stiffness conditions with varying damping are analyzed, determining optimal parameter values for the parallel combined damping NES based on trend analysis. The structure of this paper is as follows: The second section analyzes the accuracy of the harmonic balance method, the third section examines the influence of NES parameters on system vibration reduction, the fourth section investigates the optimal parameter values for NES, and the final section summarizes the main research findings of this paper.

2. Dynamic Model and Equation Establishment

This paper establishes the mechanical model of a system containing a parallel combined damping NES, as shown in Figure 1. The model consists of two parts: the main system composed of a mass block m_1, linear damping c_1, linear stiffness spring k_1, and segmented stiffness k_2. The additional parallel nonlinear energy well consists of smaller masses m_2 and m_3, linear damping c_2 and c_4, cubic stiffness k_3 and k_4 and geometric nonlinear damping c_3 and c_5 [23-24]. F(t) represents the external excitation acting on the system, x_1 denotes the displacement of the main system, and x_2 and x_3 denote the displacements of the nonlinear energy sink. For ease of description, the parallel combined damping nonlinear energy sink studied in this paper will be referred to as LG-NES.

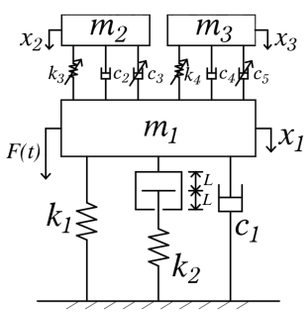

Figure 1. Mechanical Model of Segmented Linear Main System with Parallel LG-NES

The corresponding dynamic equations based on Newton's second law are established as follows:

$$\begin{cases} m_1\ddot{x}_1 + c_1\dot{x}_1 + k_1x_1 + g(x_1) + c_2(\dot{x}_1 - \dot{x}_2) + c_3(x_1 - x_2)^2(\dot{x}_1 - \dot{x}_2) + k_3(x_1 - x_2)^3 \\ \quad + c_4(\dot{x}_1 - \dot{x}_3) + c_5(x_1 - x_3)^2(\dot{x}_1 - \dot{x}_3) + k_4(x_1 - x_3)^3 = F\cos(\omega t) \\ m_2\ddot{x}_2 + c_2(\dot{x}_2 - \dot{x}_1) + c_3(x_2 - x_1)^2(\dot{x}_2 - \dot{x}_1) + k_3(x_2 - x_1)^3 = 0 \\ m_3\ddot{x}_3 + c_4(\dot{x}_3 - \dot{x}_1) + c_5(x_3 - x_1)^2(\dot{x}_3 - \dot{x}_1) + k_4(x_3 - x_1)^3 = 0 \end{cases} \tag{1}$$

The form of $g(x_1)$ in equation (1) is as follows.

$$g(x_1) = \begin{cases} k_2(x_1 - L), & x_1 > L \\ 0, & -L < x_1 < L \\ k_2(x_1 + L), & x_1 < -L \end{cases} \tag{2}$$

Here, k_2 represents the segmented linear stiffness, and L denotes the stiffness gap.

Due to the challenging nature of calculating the segmented restoring force $g(x_1)$ acting on the main system, it is approximated using a continuous function $H(x_1)$. The specific form is as follows:

$$H(x_1) = -38000k_2x_1^5 + 300k_2x_1^3 - 0.01k_2x_1 \tag{3}$$

The plot comparing $H(x_1)$ and $g(x_1)$ is shown in the figure below. Observing Figure 2, it is evident that the higher-order function demonstrates better fitting results.

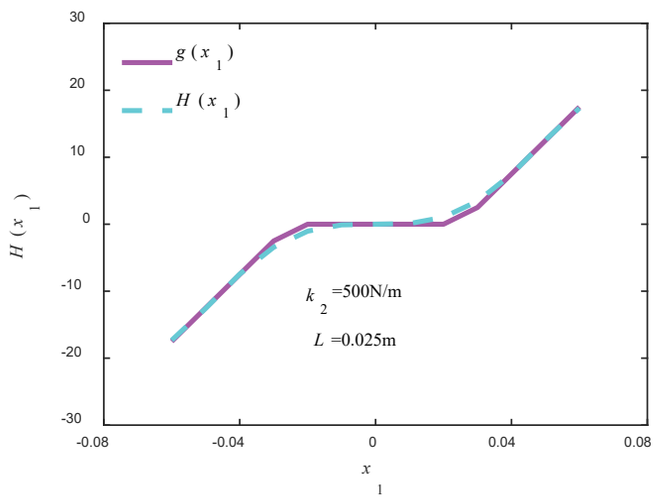

Figure 2. Comparison Between Piecewise Function and Fitted Function

The following variables are introduced to equations (1) and (3):

$$\begin{aligned}&\omega_1^2=\frac{\boldsymbol{k}_1}{\boldsymbol{m}_1},\ \lambda_i=\frac{\boldsymbol{c}_i}{\boldsymbol{m}_1\omega_1}(\boldsymbol{i}=1,2,3,4,5),\ \alpha_j=\frac{\boldsymbol{k}_j}{\boldsymbol{k}_1}(\boldsymbol{j}=2,3,4),\\&\gamma=\frac{\omega}{\omega_1},\ \varepsilon_1=\frac{\boldsymbol{m}_2}{\boldsymbol{m}_1},\ \varepsilon_2=\frac{\boldsymbol{m}_3}{\boldsymbol{m}_1},\ \boldsymbol{f}=\frac{\boldsymbol{F}}{\boldsymbol{k}_1},\ \tau=\omega_1\boldsymbol{t}\end{aligned}\tag{4}$$

Equation (1) can be transformed into:

$$\begin{cases}\ddot{x}_1+\lambda_1\dot{x}_1+x_1-38000\alpha_2x_1^5+300\alpha_2x_1^3-0.01\alpha_2x_1+\lambda_2(\dot{x}_1-\dot{x}_2)\\+\lambda_3(x_1-x_2)^2(\dot{x}_1-\dot{x}_2)+\alpha_3(x_1-x_2)^3+\lambda_4(\dot{x}_1-\dot{x}_3)\\+\lambda_5(x_1-x_3)^2(\dot{x}_1-\dot{x}_3)+\alpha_4(x_1-x_3)^3=f\cos(\gamma\tau)\\\varepsilon_1\ddot{x}_2+\lambda_2(\dot{x}_2-\dot{x}_1)+\lambda_3(x_2-x_1)^2(\dot{x}_2-\dot{x}_1)+\alpha_3(x_2-x_1)^3=0\\\varepsilon_2\ddot{x}_3+\lambda_4(\dot{x}_3-\dot{x}_1)+\lambda_5(x_3-x_1)^2(\dot{x}_3-\dot{x}_1)+\alpha_4(x_3-x_1)^3=0\end{cases}\tag{5}$$

To analyze the vibration suppression effects of the parallel LG-NES on the piecewise linear system, this study employs amplitude-frequency response curves to investigate the influence of LG-NES parameters on the system's response. According to the research by Sui et al. [25], the harmonic balance method exhibits higher accuracy in solving amplitude-frequency response. Therefore, we adopt the harmonic balance method to solve the vibration response of equation (5). Let the solution form of the equation system (5) be:

$$\begin{cases}x_1=a_{11}\cos(\gamma\tau)+b_{11}\sin(\gamma\tau)\\x_2=a_{12}\cos(\gamma\tau)+b_{12}\sin(\gamma\tau)\\x_3=a_{13}\cos(\gamma\tau)+b_{13}\sin(\gamma\tau)\end{cases}\tag{6}$$

Among them, a_{1i} and $b_{1i}(i=1,2,3)$ are the harmonic coefficients to be determined.

Substituting equation (6) into equation (5), neglecting higher-order harmonic terms, and balancing the coefficients of the $\cos(\gamma\tau)$ and $\sin(\gamma\tau)$ components, we can derive the relationship between the harmonic coefficients and the excitation frequency as follows:

$$
\begin{aligned}
&(1-\gamma^2-0.01\alpha_2)a_{11}+\gamma\left[\lambda_1 b_{11}+\lambda_2(b_{11}-b_{12})+\lambda_4(b_{11}-b_{13})\right]-23750\alpha_2 a_{11}(a_{11}^4+b_{11}^4+2a_{11}^2b_{11}^2)\\
&+225\alpha_2 a_{11}(a_{11}^2+b_{11}^2)+\left[\frac{3\alpha_3}{4}(a_{11}-a_{12})+\frac{\lambda_3\gamma}{4}(b_{11}-b_{12})\right]\left[(a_{11}-a_{12})^2+(b_{11}-b_{12})^2\right]+\\
&\left[\frac{3\alpha_4}{4}(a_{11}-a_{13})+\frac{\lambda_5\gamma}{4}(b_{11}-b_{13})\right]\left[(a_{11}-a_{13})^2+(b_{11}-b_{13})^2\right]-f=0\\
&(1-\gamma^2-0.01\alpha_2)b_{11}+\gamma\left[-\lambda_1 a_{11}+\lambda_2(a_{12}-a_{11})+\lambda_4(a_{13}-a_{11})\right]-23750\alpha_2 b_{11}(a_{11}^4+b_{11}^4+2a_{11}^2b_{11}^2)\\
&+225\alpha_2 b_{11}(a_{11}^2+b_{11}^2)+\left[\frac{3\alpha_3}{4}(b_{11}-b_{12})-\frac{\lambda_3\gamma}{4}(a_{11}-a_{12})\right]\left[(a_{11}-a_{12})^2+(b_{11}-b_{12})^2\right]+\\
&\left[\frac{3\alpha_4}{4}(b_{11}-b_{13})-\frac{\lambda_5\gamma}{4}(a_{11}-a_{13})\right]\left[(a_{11}-a_{13})^2+(b_{11}-b_{13})^2\right]=0\\
&-\varepsilon_1\gamma^2 a_{12}+\lambda_2\gamma(b_{12}-b_{11})-\left[\frac{3\alpha_3}{4}(a_{11}-a_{12})+\frac{\lambda_3\gamma}{4}(b_{11}-b_{12})\right]\left[(a_{11}-a_{12})^2+(b_{11}-b_{12})^2\right]=0\\
&-\varepsilon_1\gamma^2 b_{12}+\lambda_2\gamma(a_{11}-a_{12})-\left[\frac{3\alpha_3}{4}(b_{11}-b_{12})-\frac{\lambda_3\gamma}{4}(a_{11}-a_{12})\right]\left[(a_{11}-a_{12})^2+(b_{11}-b_{12})^2\right]=0\\
&-\varepsilon_2\gamma^2 a_{13}+\lambda_4\gamma(b_{13}-b_{11})-\left[\frac{3\alpha_4}{4}(a_{11}-a_{13})+\frac{\lambda_5\gamma}{4}(b_{11}-b_{13})\right]\left[(a_{11}-a_{13})^2+(b_{11}-b_{13})^2\right]=0\\
&-\varepsilon_2\gamma^2 b_{13}+\lambda_4\gamma(a_{11}-a_{13})-\left[\frac{3\alpha_4}{4}(b_{11}-b_{13})-\frac{\lambda_5\gamma}{4}(a_{11}-a_{13})\right]\left[(a_{11}-a_{13})^2+(b_{11}-b_{13})^2\right]=0
\end{aligned}
\tag{7}
$$

The response amplitudes of the main system and LG-NES can be expressed as:

$$
\begin{cases}
x_{1q}=\sqrt{a_{11}^2+b_{11}^2}\\
x_{2q}=\sqrt{a_{12}^2+b_{12}^2}\\
x_{3q}=\sqrt{a_{13}^2+b_{13}^2}
\end{cases}
\tag{8}
$$

Using the Matlab software to solve the nonlinear equation system (7) and substituting the results into equation (8) will provide the outcomes obtained using the harmonic balance method. Simultaneously, applying the Runge-Kutta method to solve equation (1) allows for numerical validation of the accuracy of the solutions derived from the harmonic balance method. The system parameters [26] are selected as shown in the table below.

Table 1. System Parameters

Parameter	Value	Unit
m_1	3	Kg
m_2	0.15	Kg
m_3	0.15	Kg
c_1	5	Ns/m
c_2	5	Ns/m
c_3	5	Ns/m
c_4	5	Ns/m
c_5	5	Ns/m
k_1	1×10^4	N/m
k_2	500	N/m
k_3	1×10^4	N/m
k_4	1×10^4	N/m
F	20	N

Based on the parameters in Table 1, plot the amplitude-frequency response curves for the piecewise linear main system and LG-NES as shown in Figure 3.

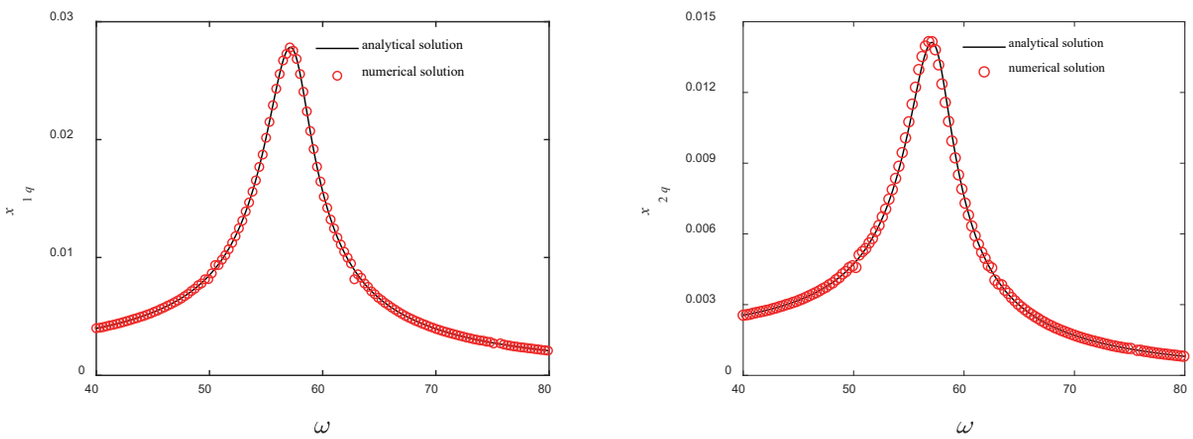

(a) Main system **(b) Nonlinear energy sink**

Figure 3. Comparison between Analytical and Numerical Solutions of Amplitude-Frequency Response

As both LG-NES parameters share the same values and are connected in parallel, Figure 3 displays the amplitude-frequency response curve for only one of the LG-NES units. From Figure 3, it is evident that there is good agreement between the numerical and analytical solutions, confirming the accuracy of the harmonic balance method in solving the system.

3. Vibration Reduction Performance Analysis

Next, we will analyze the effects of LG-NES mass, stiffness, and damping on the vibration suppression of the main system. As the nonlinear energy sinks in this study are connected in parallel and have the same initial parameter values, both nonlinear energy sinks contribute equally to the vibration reduction effect on the main system. Therefore, in the subsequent analysis of parameter effects, we maintain consistent changes in the parameters of the two LG-NES units.

3.1 Influence of LG-NES Mass

This subsection analyzes the impact of LG-NES mass on the amplitude-frequency response of the main system. The parameters remain consistent with those in Table 1. We will plot the amplitude-frequency response for different LG-NES masses under various external excitations F and the coupled amplitude-frequency response of a single LG-NES, where the mass of a single LG-NES is 0.3 kg, as shown in Figure 4.

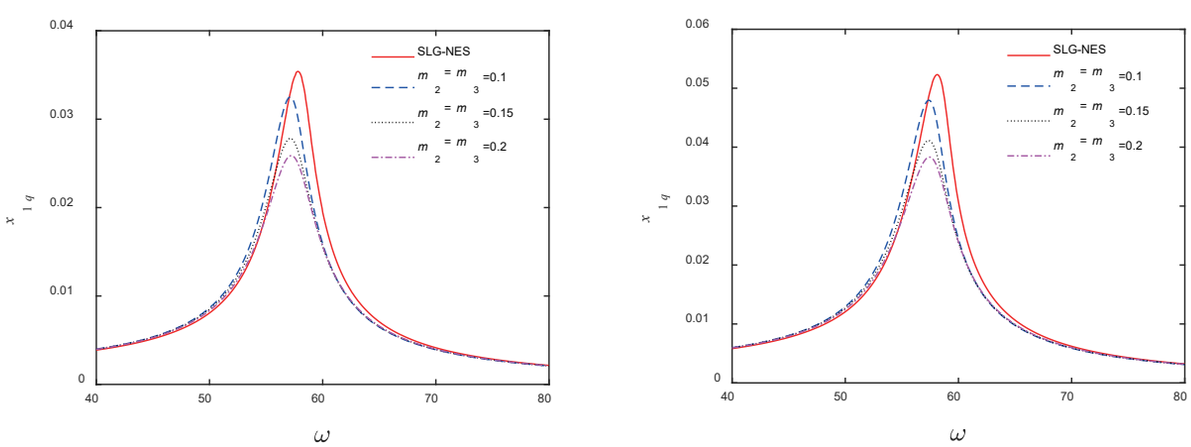

(a) F **= 20N** **(b)** F **= 30N**

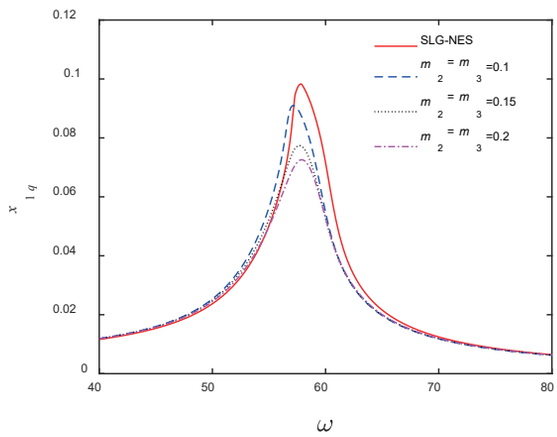

(c) $F = 60$N

Figure 4. Amplitude-Frequency Response Curves of the Main System for Different Masses and Excitation Amplitudes

The SLG-NES in the figure represents a single connected LG-NES. As seen in Figure 4, when the additional LG-NES masses are equal, the resonance amplitude of the parallel LG-NES is lower than that of the single connected LG-NES. This demonstrates that the parallel connection effectively reduces the resonance amplitude of the main system. Moreover, it's observed that the resonance amplitude of the main system decreases with increasing additional mass. This indicates that increasing the additional mass of the NES can enhance the vibration reduction performance of the LG-NES on the main system.

To further analyze the impact of LG-NES mass on the vibration suppression of the main system, plotting the trend of the maximum amplitude A at resonance against the LG-NES mass is presented in the following figure, where 'PLG-NES' signifies the parallel connected LG-NES.

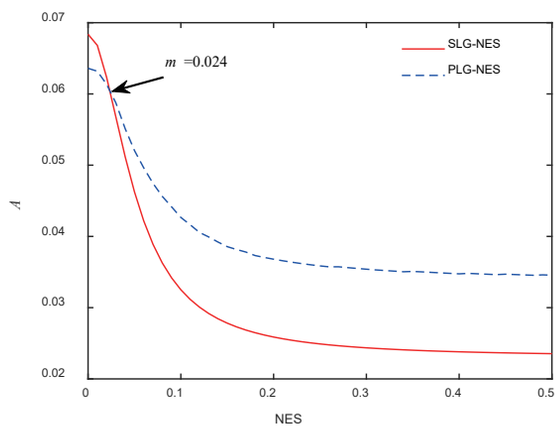

Figure 5. Variation of Maximum Amplitude with LG-NES Mass

From Figure 5, it is observed that after the LG-NES mass reaches 0.024, the maximum amplitude corresponding to the parallel connection is lower than that of the single connected LG-NES. In other words, the parallel connection performs better in vibration reduction than connecting a single NES for most masses. Additionally, it's noticed that after reaching a certain additional mass, the trend of the maximum amplitude tends toward a straight line. At this point, the increase in mass has minimal impact on the vibration reduction effect.

Therefore, considering that the additional NES mass should not be too high to avoid increasing the burden on the main system, $m_2 = m_3 = 0.15$Kg is chosen, a mass ratio of 0.1 for the subsequent analysis.

3.2 Influence of LG-NES Stiffness

Next, the effect of LG-NES stiffness on the amplitude-frequency response of the piecewise linear main system is analyzed. Based on the conclusion from 3.1, choosing $\boldsymbol{m_2 = m_3 = 0.15\mathbf{Kg}}$, while keeping the other parameters consistent with Table 1, amplitude-frequency response curves for different k_{NES} values are plotted for both parallel and single connections, as shown in Figure 6. SLG-NES in the figure represents a single connected LG-NES, while PLG-NES denotes the parallel connected LG-NES.

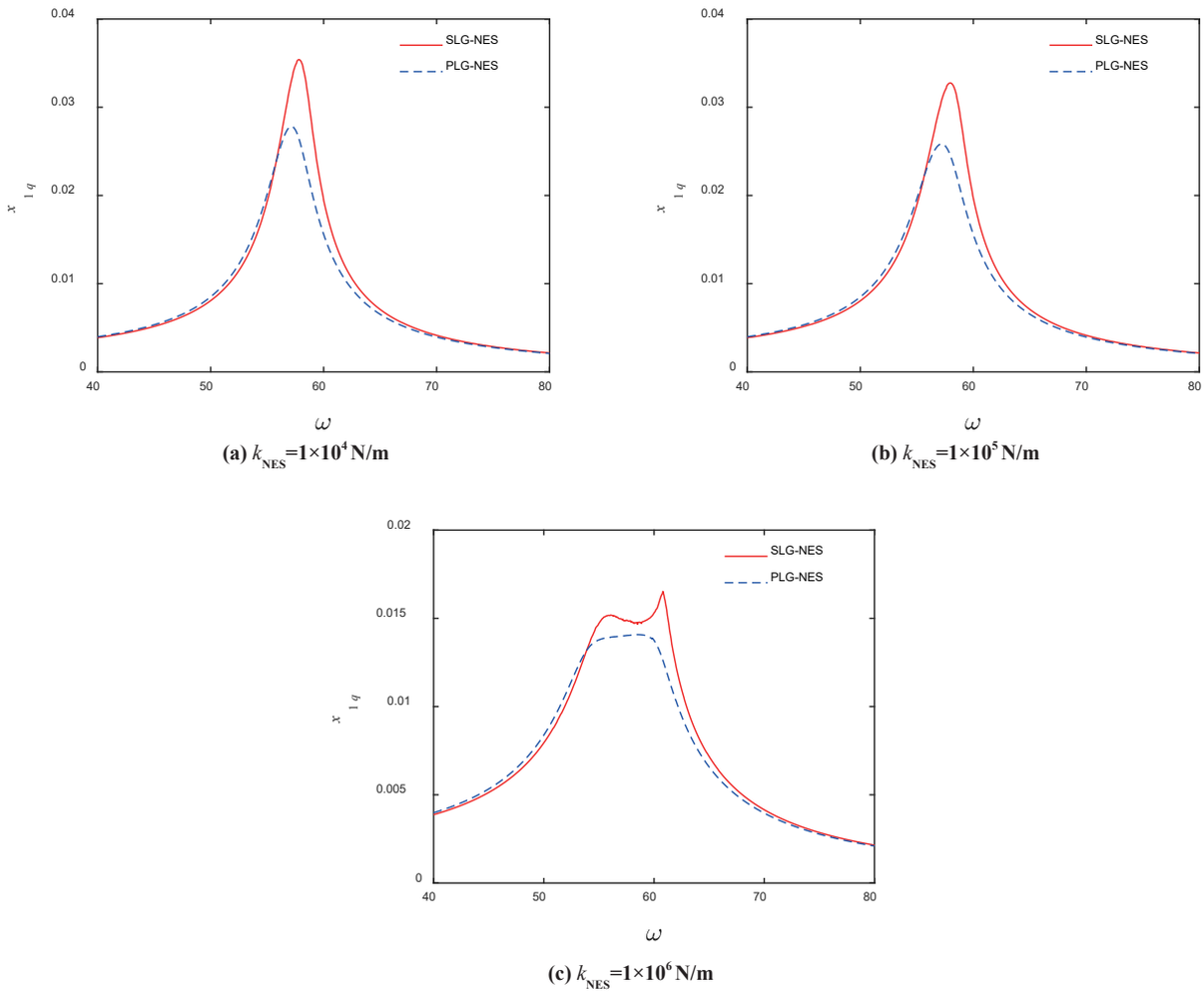

Figure 6. Comparison of Vibration Reduction Performance between Parallel LG-NES and Single Connected LG-NES under Different k_{NES} Values

From Figure 6, it's evident that at the same stiffness, the parallel connection effectively reduces the resonance amplitude of the piecewise linear main system. Additionally, it is observed that as the LG-NES stiffness increases, the LG-NES exhibits a better vibration suppression effect on the main system.

To more precisely illustrate the trend of vibration reduction performance of the parallel LG-NES concerning k_{NES} variations, Figure 7 and Figure 8 respectively present the amplitude-frequency response curves and the time response of the main system at resonance frequency with changes in the stiffness of the nonlinear energy sink for the parallel connection.

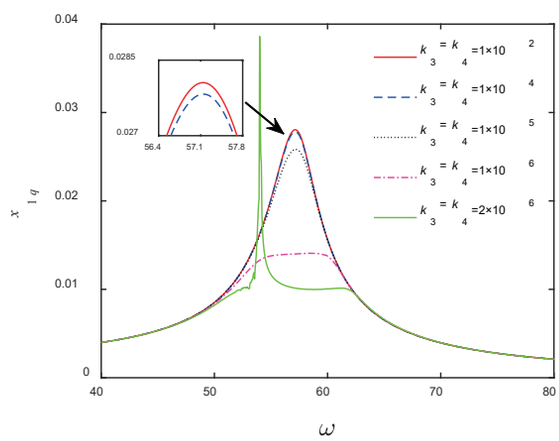

Figure 7. Variation of Main System's Amplitude-Frequency Response with k_{NES}

From Figure 7, it can be observed that within a certain range of stiffness coefficients of the nonlinear energy sink, the peak of the main system's amplitude-frequency response curve decreases as the stiffness coefficient increases. This indicates an improvement in the vibration suppression effect of the LG-NES. As depicted in Figure 8(a) and Figure 8(b), selecting an appropriate stiffness enhances the LG-NES's vibration reduction effect. Moreover, from Figure 8(b), it can be noted that when the stiffness is chosen as 1×10^6 N/m, the main system exhibits strongly modulated responses near the resonance frequency. This modulation significantly adjusts the amplitude of the main system's response, effectively reducing its vibration amplitude. However, when the stiffness coefficient is excessively high, as shown in Figure 8(c), a resonance peak appears at $\omega = 54$ in the amplitude-frequency response. At this point, the vibration amplitude of the main system is higher than that observed with a smaller stiffness, which is unfavorable for the LG-NES in reducing the main system's vibrations.

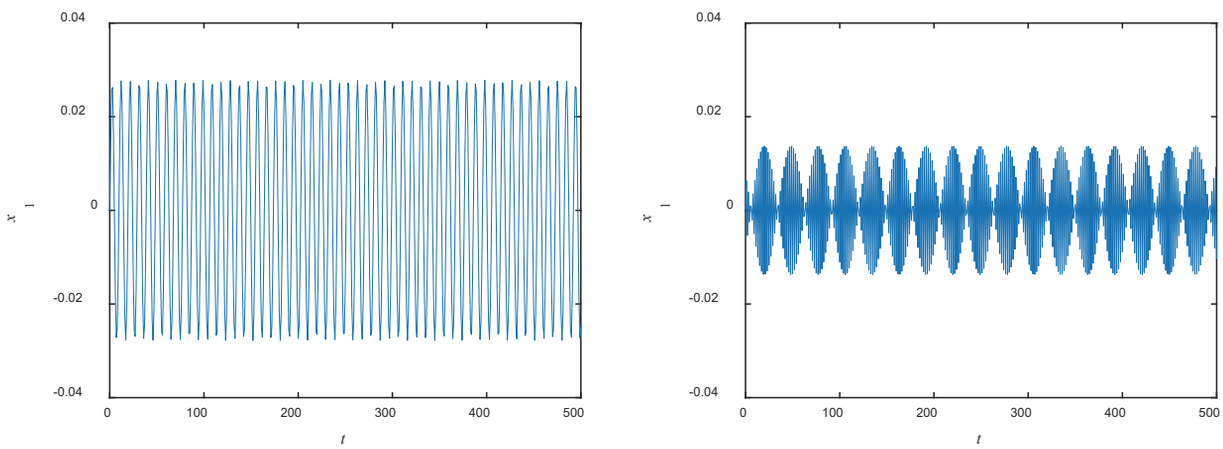

(a) k_{NES}**=1×10⁴ N/m** **(b)** k_{NES}**=1×10⁶ N/m**

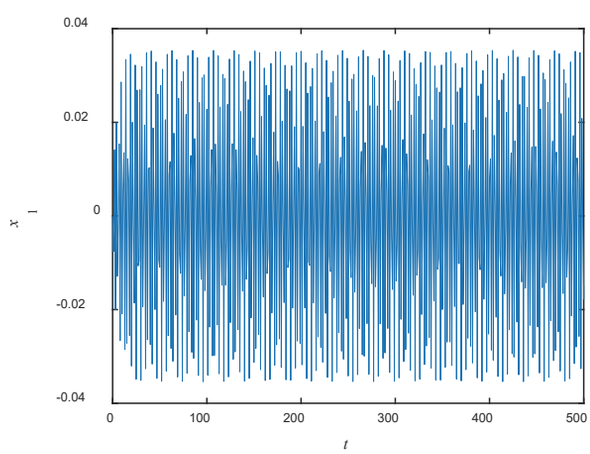

(c) k_{NES}**=2×10⁶ N/m**

Figure 8. Time Response at Different Resonant Frequencies with Varied k_{NES}

Following the above analysis, when the stiffness of the nonlinear energy sink is excessively high, it causes abnormal peaks in the amplitude-frequency response of the main system. To avoid such occurrences, the trend of the maximum amplitude A concerning the stiffness variation of the nonlinear energy sink is plotted, as shown in the following figure.

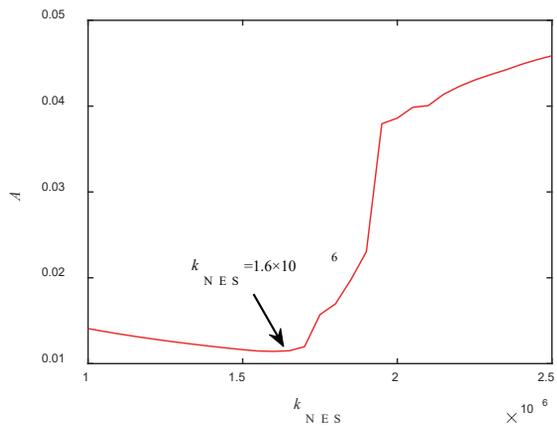

Figure 9. Variation of Maximum Amplitude with LG-NES Stiffness

Observing Figure 9, it can be noticed that when the stiffness of the nonlinear energy sink is less than 1.6×10^6 N/m, the maximum amplitude A decreases with an increase in stiffness. However, when it exceeds 1.6×10^6 N/m, the maximum amplitude A sharply rises, which is unfavorable for vibration reduction in the main system.

From the above analysis, it is evident that when designing the LG-NES, an appropriately high stiffness should be chosen to reduce the resonance amplitude and bandwidth of the main system, enabling the nonlinear energy sink to exert optimal vibration reduction performance.

3.3 Influence of LG-NES Damping

Finally, we analyze the impact of damping on the amplitude-frequency response of the main system. For descriptive purposes, define the ratio of the geometric nonlinear damping to linear damping for the two LG-NES as β_1 and β_2, respectively. Using the same parameters as before, amplitude-frequency responses for different damping values under $\beta_1 = \beta_2 = 1$ are plotted in Figure 10.

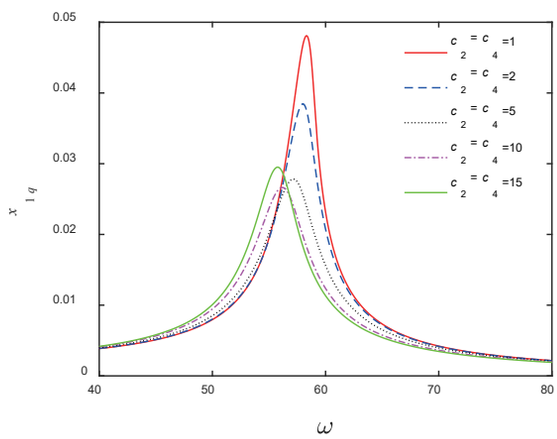

Figure 10. Variation of Main System's Amplitude-Frequency Response with Damping

From Figure 10, it is evident that when the damping ratio remains constant, within a specific range of damping values, the peak of the main system's amplitude-frequency response decreases with increasing damping. However, when the damping value is 15, the peak of the amplitude-frequency response increases instead. This indicates the presence of an optimal damping value that minimizes the resonance amplitude of the main system.

To determine the appropriate damping coefficient, the following figure illustrates the variation of the maximum amplitude of the main system concerning the damping in $\beta_1 = \beta_2 = 1$.

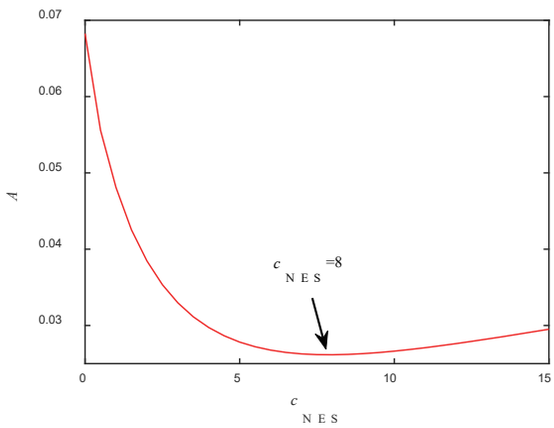

Figure 11. Variation of Maximum Amplitude with LG-NES Damping

From Figure 11, it is observed that at $\beta_1 = \beta_2 = 1$, when the damping value is 8 Ns/m, the peak of the amplitude-frequency response is minimized, indicating the main system achieves optimal vibration reduction.

The analysis regarding the damping coefficient only considered $\beta_1 = \beta_2 = 1$. To find an appropriate damping ratio, comparative graphs illustrating the resonance amplitude of the main system under different damping ratios and the variation of the maximum amplitude concerning the damping ratio will be plotted separately.

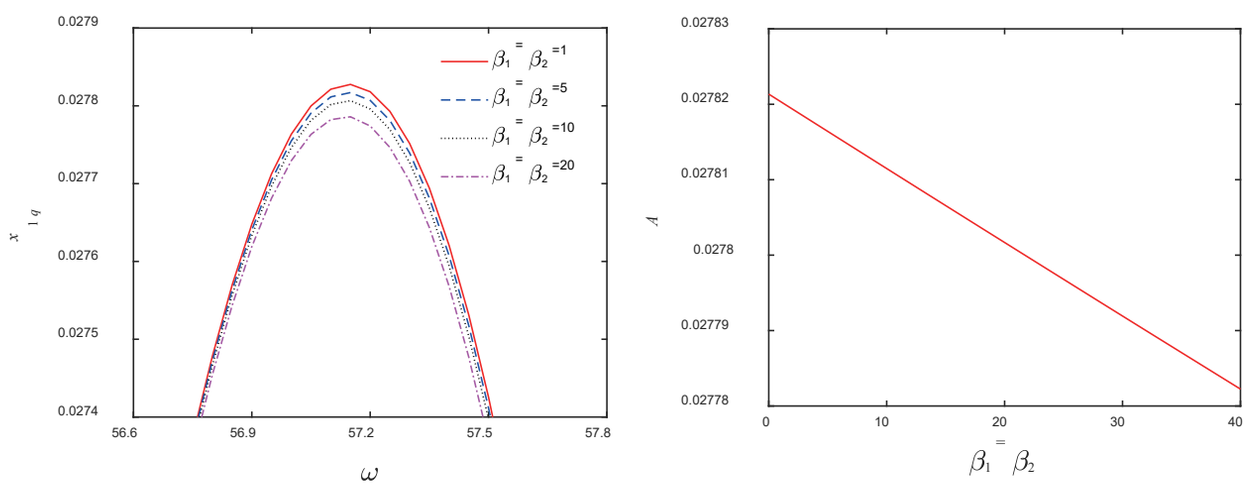

(a) Variation of Peak Amplitude in Amplitude-Frequency Response with Damping Ratio

(b) Variation of Maximum Amplitude with Damping Ratio

Figure 12. Amplitude Variation under Different Damping Ratios

From Figure 12, it's evident that the larger the ratio between geometric nonlinear damping and linear damping, the lower the maximum amplitude in the amplitude-frequency response of the main system. This suggests that the vibration reduction capability of LG-NES is directly proportional to the damping ratio. In other words, a larger chosen damping ratio results in better vibration reduction effects for the main system. In summary, when designing LG-NES, one should opt for a larger NES mass, appropriately sized NES stiffness, and a higher damping ratio to ensure the segmented linear main system attains optimal vibration reduction effects.

4. Parameter Optimization

As per the findings from the second part, the analysis of LG-NES parameters on the system's frequency response has been conducted, yielding the optimal additional NES mass and optimal damping ratio. Next, by altering the LG-NES damping, three-dimensional graphs illustrating the changes in frequency response with damping for different stiffness values will be plotted, along with a graph depicting the variation in maximum response amplitude. This will aid in identifying the best range of values for stiffness and damping.

The selected parameters are as follows: total mass chosen as 0.3 kg, damping ratio set at 10, and stiffness taken as 1×10^4 N/m, 1×10^5 N/m, 1×10^6 N/m, and 1×10^6 N/m respectively. By varying the damping coefficient, a set of graphs will be generated illustrating the frequency response of the main system and the trends in maximum response amplitude for different stiffness values.

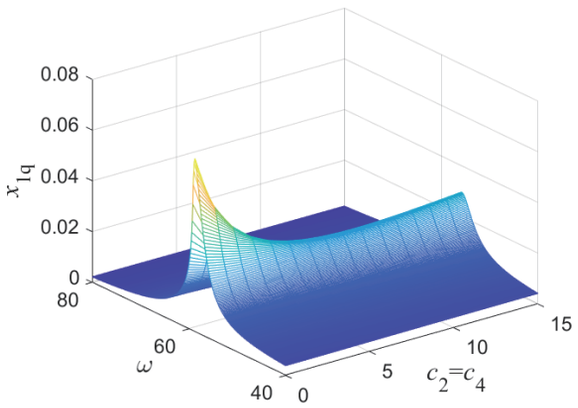

(a) k_{NES}=1×10^4 N/m

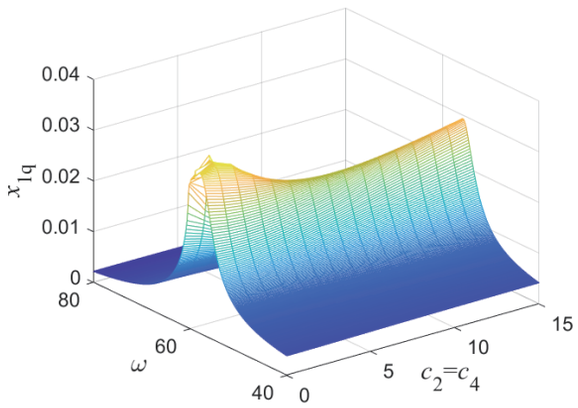

(b) k_{NES}=1×10^5 N/m

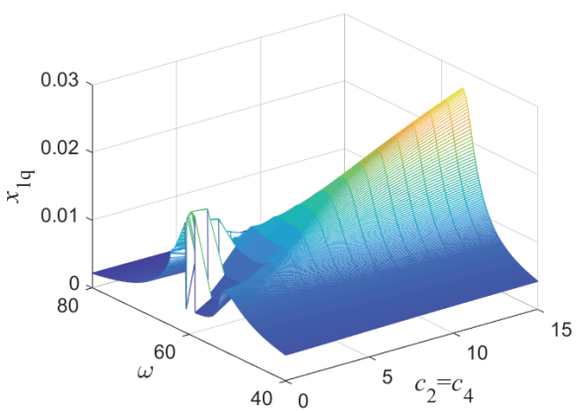

(c) k_{NES}=1×10^6 N/m

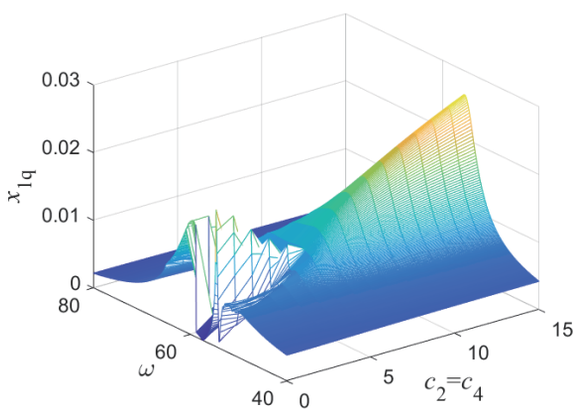

(d) k_{NES}=1.6×10^6 N/m

Figure 13. Three-Dimensional Graph of Frequency Response Changes with Damping for Different Stiffness Values

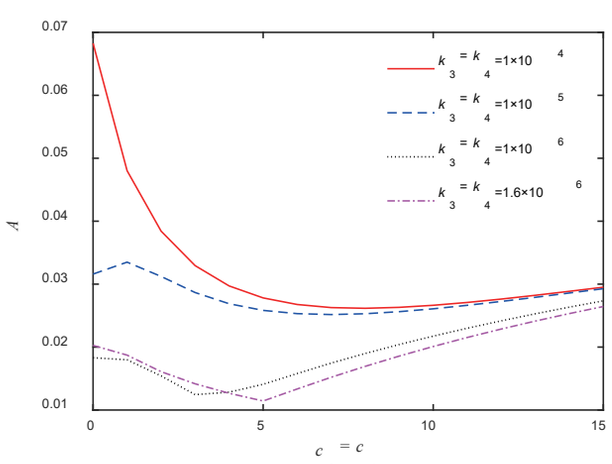

Figure 14. Three-Dimensional Graph of Frequency Response Changes with Damping for Different Stiffness Values

From Figures 13 and 14, it is evident that the optimal range for damping varies with different stiffness values. The vibration damping effect of the nonlinear energy sink (NES) on the main system also differs accordingly. When the stiffness is 1×10^4 N/m the optimal damping value is 8 Ns/m, resulting in a maximum response amplitude of 0.026 for the main system. As the stiffness increases to 1×10^5 N/m, the optimal damping value decreases to 7 Ns/m, with the maximum response amplitude reaching 0.025. However, when the stiffness is further increased to 1×10^6 N/m and 1.6×10^6 N/m, the main system exhibits a phenomenon of strongly modulated response. At these stiffness levels, the maximum response amplitude notably decreases to 0.012 and 0.011, respectively, with damping values of 3 Ns/m and 5 Ns/m, indicating a significant vibration reduction effect. Based on this analysis, the final determined parameter values are as follows: total NES mass of 0.3 Kg, NES stiffness of 1.6×10^6 N/m, NES linear damping of 5 Ns/m, and a damping ratio of 10.

Based on the obtained optimal parameters, a comparison of the frequency response before and after optimization is shown in Figure 15 below. From Figure 15, it is evident that after optimization, there is a significant reduction in response amplitude, enhancing the vibration damping performance of the LG-NES and providing the main system with improved vibration reduction effects.

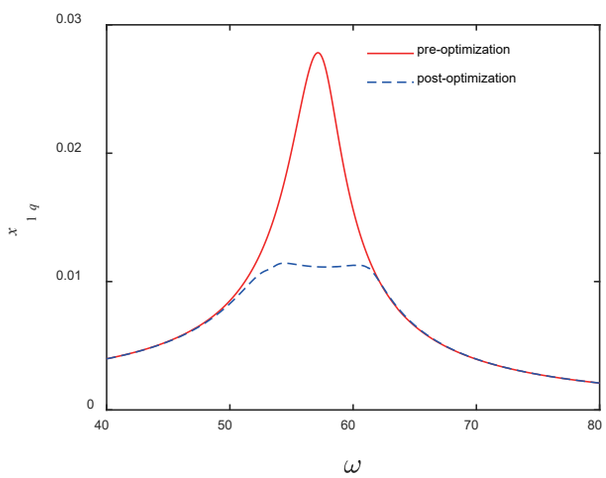

Figure 15. Comparison of the main system's frequency response before and after optimization.

5. Conclusion

This paper introduces parallel LG-NES for segmented linear systems and analyzes its vibration suppression effect under harmonic excitation. Firstly, a fitting process was performed on the segmented function. The frequency response of the system was then determined using the harmonic balance method and verified using the Runge-Kutta method to confirm its accuracy. Secondly, the impact of various LG-NES parameters on the main system's vibration damping was analyzed, and values for mass and damping ratio were established. Subsequently, the change in the main system's response amplitude trend when the damping changes under different stiffness values was investigated, determining the values for stiffness and damping, and comparing the optimized vibration reduction effect. The specific conclusions are as follows:

(1) Compared to a single connection, a parallel connection allows the main system to achieve better vibration reduction under harmonic excitation. As the additional NES mass increases, the main system's resonance amplitude continues to decrease. However, after reaching a mass of 0.3Kg, the maximum response amplitude change approximates a straight line. At this point, increasing the mass does not improve the nonlinear energy trap's vibration reduction performance.

(2) With an increase in stiffness, the main system's resonance amplitude consistently decreases. However, when the stiffness value becomes excessively large, the main system's frequency response shows abnormal peaks, which are unfavorable for vibration reduction. As the damping ratio increases, the main system's resonance amplitude also decreases consistently, albeit to a lesser extent. Therefore, selecting a moderately high damping ratio suffices.

(3) As the damping increases, the maximum response amplitude of the main system initially decreases and then rises. Additionally, it was observed that when stiffness changes, the optimal damping value for achieving the best vibration reduction effect also changes. Through a comparison of trends in the maximum amplitude with damping under different stiffness values, it was concluded that when the stiffness is 1.6×10^6 N/m and the damping is 5Ns/m, the main system achieves optimal vibration reduction. Lastly, a comparison of the frequency response before and after optimization was presented.

References

[1] Balaji P S, Karthik SelvaKumar K. Applications of nonlinearity in passive vibration control: a review[J]. Journal of Vibration Engineering & Technologies, 2021, 9: 183-213.

[2] Lu Z, Wang Z, Zhou Y, et al. Nonlinear dissipative devices in structural vibration control: A review[J]. Journal of Sound and Vibration, 2018, 423: 18-49.

[3] Tehrani G G, Dardel M, Pashaei M H. Passive vibration absorbers for vibration reduction in the multi-bladed rotor with rotor and stator contact[J]. Acta Mechanica, 2020, 231: 597-623.

[4] Charlemagne S, Lamarque C H, Savadkoohi A T. Dynamics and energy exchanges between a linear oscillator and a nonlinear absorber with local and global potentials[J]. Journal of Sound and Vibration, 2016, 376: 33-47.

[5] Sarmeili M, Ashtiani H R R, Rabiee A H. Nonlinear energy sinks with nonlinear control strategies in fluid-structure simulations framework for passive and active FIV control of sprung cylinders[J]. Communications in Nonlinear Science and Numerical Simulation, 2021, 97: 105725.

[6] Saeed A S, Abdul Nasar R, AL-Shudeifat M A. A review on nonlinear energy sinks: designs, analysis and applications of impact and rotary types[J]. Nonlinear Dynamics, 2023, 111(1): 1-37.

[7] Ding H, Chen L Q. Designs, analysis, and applications of nonlinear energy sinks[J]. Nonlinear Dynamics, 2020, 100(4): 3061-3107.

[8] Wang J, Wang B, Wierschem N E, et al. Dynamic analysis of track nonlinear energy sinks subjected to simple and stochastice excitations[J]. Earthquake Engineering & Structural Dynamics, 2020, 49(9): 863-883.

[9] Li H, Li A, Kong X. Design criteria of bistable nonlinear energy sink in steady-state dynamics of beams and plates[J]. Nonlinear Dynamics, 2021, 103(2): 1475-1497.

[10] Zang J, Cao R Q, Zhang Y W. Steady-state response of a viscoelastic beam with asymmetric elastic supports coupled to a lever-type nonlinear energy sink[J]. Nonlinear Dynamics, 2021, 105: 1327-1341.

[11] Chen J E, Sun M, Hu W H, et al. Performance of non-smooth nonlinear energy sink with descending stiffness[J]. Nonlinear Dynamics, 2020, 100: 255-267.

[12] Geng X F, Ding H, Mao X Y, et al. Nonlinear energy sink with limited vibration amplitude[J]. Mechanical Systems and Signal Processing, 2021, 156: 107625.

[13] Wang G X, Ding H, Chen L Q. Performance evaluation and design criterion of a nonlinear energy sink[J]. Mechanical Systems and Signal Processing, 2022, 169: 108770.

[14] Yang T, Hou S, Qin Z H, et al. A dynamic reconfigurable nonlinear energy sink[J]. Journal of Sound and Vibration, 2021, 494: 115629.

[15] Ji J C, Zhang N. Suppression of the primary resonance vibrations of a forced nonlinear system using a dynamic vibration absorber[J]. Journal of Sound and Vibration, 2010, 329(11): 2044-2056.

[16] Piccirillo V. Suppression of chaos in nonlinear oscillators using a linear vibration absorber[J]. Meccanica, 2021, 56(2): 255-273.

[17] Wang Y, Li X, Shen Y. Vibration reduction mechanism of Van der Pol oscillator under low-frequency forced excitation by means of nonlinear energy sink[J]. International Journal of Non-Linear Mechanics, 2023, 152: 104389.

[18] Dang W, Wang Z, Chen L Q, et al. A high-efficient nonlinear energy sink with a one-way energy converter[J]. Nonlinear Dynamics, 2022, 109(4): 2247-2261.

[19] Bab S, Khadem S E, Shahgholi M, et al. Vibration attenuation of a continuous rotor-blisk-journal bearing system employing smooth nonlinear energy sinks[J]. Mechanical Systems and Signal Processing, 2017, 84: 128-157.

[20] Kong X, Li H, Wu C. Dynamics of 1-dof and 2-dof energy sink with geometrically nonlinear damping: application to vibration suppression[J]. Nonlinear Dynamics, 2018, 91: 733-754.

[21] Song W, Liu Z, Lu C, et al. Analysis of vibration suppression performance of parallel nonlinear energy sink[J]. Journal of Vibration and Control, 2023, 29(11-12): 2442-2453.

[22] Zhang Y, Kong X, Yue C, et al. Dynamic analysis of 1-dof and 2-dof nonlinear energy sink with geometrically nonlinear damping and combined stiffness[J]. Nonlinear Dynamics, 2021, 105(1): 167-190.

[23] Andersen D, Starosvetsky Y, Vakakis A, et al. Dynamic instabilities in coupled oscillators induced by geometrically nonlinear damping[J]. Nonlinear Dynamics, 2012, 67: 807-827.

[24] Andersen D K, Vakakis A F, Bergman L A. Dynamics of a system of coupled oscillators with geometrically nonlinear damping[C]//Nonlinear Modeling and Applications, Volume 2: Proceedings of the 28th IMAC, A Conference on Structural Dynamics, 2010. New York, NY: Springer New York, 2011: 1-7.

[25] Sui P, Shen Y J, Wang X N. A Comparison of Complex Variable Averaging Method and Other Approximation Techniques[J]. Journal of Vibration and Shock, 2023, 42(10): 289-296. DOI: 10.13465/j.cnki.jvs.2023.10.034.

[26] Geng X F, Ding H. Two-modal resonance control with an encapsulated nonlinear energy sink[J]. Journal of Sound and Vibration, 2022, 520: 116667.